Generation and Propagation of Nano Shock Waves in a Lennard-Jones Fluid

A Thesis Submitted to
The Department of Physics
College of Natural & Computational Sciences
Addis Ababa University

In Partial Fulfilment of
the Requirement for the Degree
of Master of Science in Physics (Statistical Physics)

by

Kidanemaryam Shambel Belew

Advisor:

Tatek Yirgu (Associate Professor of Physics)

Addis Ababa, Ethiopia
August 2021

Addis Ababa University
College of Natural & Computational Science
Department of Physics

Submitted by:

Kidanemaryam Shambel Signature ..... Date .....

This is to certify that the thesis prepared by Kidanemaryam Shambel, entitle **"Generation and Propagation of Nano Shock Waves in a Lenard-Jones Fluid"** submitted in partial Fulfillment of the requirement for the degree of master of Sciences in physics (Statistical Physics) complies with the regulation of the University and meets the the accepted standards with respect to originality.

Approved by the Examination Committee

Dr. Tatek Yirgu (Advisor)	(Signature and Date)	(Date)
Dr. Mulugeta Bekele (Examiner)	(Signature)	(Date)
Dr. Lemi Demeyu (Examiner)	(Signature)	(Date)
Dr. Teshome Senbeta (Chairman)	(Signature)	(Date)

To the Beloved

Acknowledgment

This work has been supported in part by The International Science Program (ISP), Uppsala University, Sweden.

Abstract

A three-dimensional Molecular Dynamics simulation (MD) is implemented to grasp an insightful understanding of shock wave propagation on a nanoscale. Primarily, we have reviewed some of its potential uses in medical and biological areas. Mainly, we have come across reviewing some experimental investigations on a (mm-cm) scale. Some of the results show that as the shock wave's strength decreases rapidly, so does its amplitude and velocity. According to our simulation results the asymptotic variance of wave amplitude and speed have been perfectly correlated. Furthermore, in correspondence to some experimental results [1, 2], we have found that the pressure pulse-amplitude is proportional to the power of the distance from the source ($\Delta P_a \sim \zeta^m$). Correspondingly, the displacement pulse-amplitude also shows similar characteristics ($\Delta z_a \sim \zeta^m$).

Contents

List of Figures

List of Tables

"If nature were not beautiful, it would not be worth studying it. And life would not be worth living."

— Henry Poincaré

1 Introduction

1.1 Shock waves and their characteristics

To begin with, when a powerful perturbation happens in a medium such as gas, liquid and solid, it causes compression to occur in a region whereby a sudden change in temperature, stress and density generates high-speed traveling mechanical wave, namely shock waves. By definition, shock waves are discontinuous phenomena and are felt by our senses as a sudden and violent event. A shock wave is a transient pressure disturbance that propagates rapidly in three-dimensional space. They are also audible high-energy sound waves or the propagation of disturbance that travels at a supersonic speed and faster than the local speed of sound in the medium. Accordingly, a sonic boom phenomenon is a peculiar characteristic of shock waves, in which a bang sound is heard when objects travel faster than the speed of sound. Usually, they are characterized by a sudden rise from ambient pressure to its maximum pressure. We also observe that their amplitude decays at much faster rate than $\sim 1/r$ in water [3], where r denotes the distance from the source. Most often, one can observe a shock wave while detonation is taking place. A detonation wave is a supersonic combustion wave across which the thermodynamic variables (e.g., pressure and temperature) increase sharply [4].

Furthermore, all kinds of violent phenomena in nature extends from terrestrial to cosmic dimension, can be attributed to the consequence of the shock wave process [5]. Among many other causes for the generation of a shock wave is void collapse. A traveling shock signal with negative pressure amplitude leaves a bubble (cavity) through which it propagates; hence moments later, it implodes and causes a secondary shock to occur. Concernedly, shock waves generated by underwater explosions have been observed to cause the dissemination of aquatic animals. A recent project undertaken in Wilmington Harbor, North Carolina, showed that propagation of shock impulse that ranges from 1.855 to 12.080 Pa s could kill a substantial number of larvae in a nearby area to the explosion. [6]. Moreover, the implosion of nano-bubbles created as a consequence of shock wave passage in living tissue could cause a series of damages or even destruction on the blood-brain barrier [7].

1.2 Applications of shock waves

In the medical arena, shock waves have been playing a crucial role in the diagnosis of multiple anatomical problems. The treatment is given using an extracorporeal shock wave, by which a shock wave is generated outside the body, and travels through the patient skin into the tissue. In orthopedics, shock waves are used to treat insertional tendinopathies and bone fractures [7, 8]. Additionally, Shock Wave Lithotripsy (SWL) is the most common treatment in the area of Urology for the disintegration of renal calculi (kidney stones) [9]. Interestingly, it has been also used for the disintegration of gallbladder stones [10]. Moreover, according to some studies, extracorporeal shock-wave therapy (ESWT) has been able to show a bactericidal effect [11–13]. As stated by article [14], a spherical micro-shock wave could be used for gene treatment, food preservation, particle delivery systems, and many more novel applications in the discipline of Biology. These and many application areas clearly show a great deal of concern has to be given in the area of shock-wave investigation.

1.3 Shock wave investigations

For the last few decades, the generation and propagation of underwater shock waves have been studied through different techniques. The piezoelectric effect has been widely used

in various under-water shock wave studies [15, 16], it enables to measure perturbation amplitude, characterized by a narrow pulse and sharp pressure peak, which lasts for a few microseconds. Most often underwater electrical discharge is capable of generating strong shock waves (SSWs) [17, 18]. Accordingly, pressure amplitude of the shock waves can be measured using piezoelectric pressure prob, which is most frequently placed at a few centimeters away from the shock source, while the characteristic curves are filtered through the signal processing algorithm method, which depends upon energy conservation requirement and Fourier analysis [18]. Besides, shock waves can be generated using a laser. When a pulsed laser shine over certain absorbing material, there occurs deposition of optical energy. Consequently, the conversion of stored optical energy into mechanical energy could lead to the generation and propagation of shock waves at the surface [19]. Varying laser fluence (total energy deposited per unit area of illumination), enables one to control pick stress of propagation [20–22]. A recent experimental examination reveals that laser-induced underwater shock waves give a symmetrical pressure impulse for a wide range of experimental parameters in proximity. Interestingly, the same event can be seen when the shock waves are generated at an elongated region [23]. However, many experimental results assess shock waves in the order of a few microseconds time scale of rise and fall of the pressure pulse.

Due to the unavailability of experimental tools that could enable shock waves investigation in a nano-time scale, a numerical analysis has been alternatively used for many decades. Studies on such a minute scale may provide us enough information regarding how organic molecules react to the incident shock. In fact, some kind of perturbation that happens in the water molecules could result in a shock wave, hence an inevitable impact on the structure of organic molecules will be observed. Accordingly, a recent article showed that a shock wave-induced damage on a Protein by Void Collapse using a Molecular dynamics simulation [24]. In addition, there has been a study carried out in order to understand the mechanism of membrane poration by shock wave induced nano-bubble collapse using the same simulation technique [25]. Further, a related study shows that substantial damage on the phospholipid membrane could be observed if the shock wave is created in the vicinity [26].

There have been attempts to simulate shock waves in solids, liquids, and dense gases using the direct simulation Monte Carlo method and the Molecular Dynamics (MD)[27–35]. The MD method has been applied almost exclusively in the simulation of shocks in liquids and solids. In these computations, Maxwellian molecules or Lennard-Jones

molecules are typically used as a choice for inter-molecular force laws. And the shock wave is generally created by moving a plane of atoms at one side of the simulation volume with a constant piston velocity or by altering conditions at two opposing sides so that a stationary shock is established within the simulation box. Shock wave simulations are frequently accompanied by solitary waves which have been observed first in one dimension and generalized into three dimensions [36–38]. In a recent experimental investigation, in-depth insight into the structure of shock wave has been achieved in ($mm - cm$) scale, with a variety of shock profile [15, 17, 39–42]. In particular, the spatial and temporal variation of shock wave amplitude, as well as time-dependent velocity of propagation, have been motivated us to see if there could be a resemblance, even down to a nano-scale.

The rest of the paper is organized as follows: in Section 2, we present the simulation model, in Section 3, we put our simulation results, and discussion is made, accordingly. Finally, in Section 4, we put forth a concluding remark.

2
Methods

2.1 Simulation setup

First we set up a three dimensional simulation box of size $(L_x \times L_y \times L_z) = (70 \times 70 \times 140)\sigma$, where σ is the length parameter, and then particles were initially ordered in a face-centered cubic (fcc) crystal structure inside the box. The reason is for simulation of fluids, it is convenient to start with the particles in a perfect fcc crystal and prepare the system at high temperature, after few steps our crystal melts and we obtain a liquid. Consequently, the initial velocity of the particles is assigned using Maxwell-Boltzmann distribution for a working temperature of $94.0K$. To minimize edge effects and thereby model an infinite system, a periodic boundary condition is applied in all directions of the simulation box. We have used $405,224$ particles placed inside 168 planes in the simulation box, formed in the $x-y$ plane, and ordered along the z-direction. Each plane is $L_z/168\sigma$ thick and holds around $2,412$ particles. The overall simulation setup is shown in the schematic diagram shown in Figure 2.1. Conveniently, we have considered an NVE micro-canonical ensemble for incompressible fluid. The system is isolated so that there will not be an exchange of energy or particle with the outside environment.

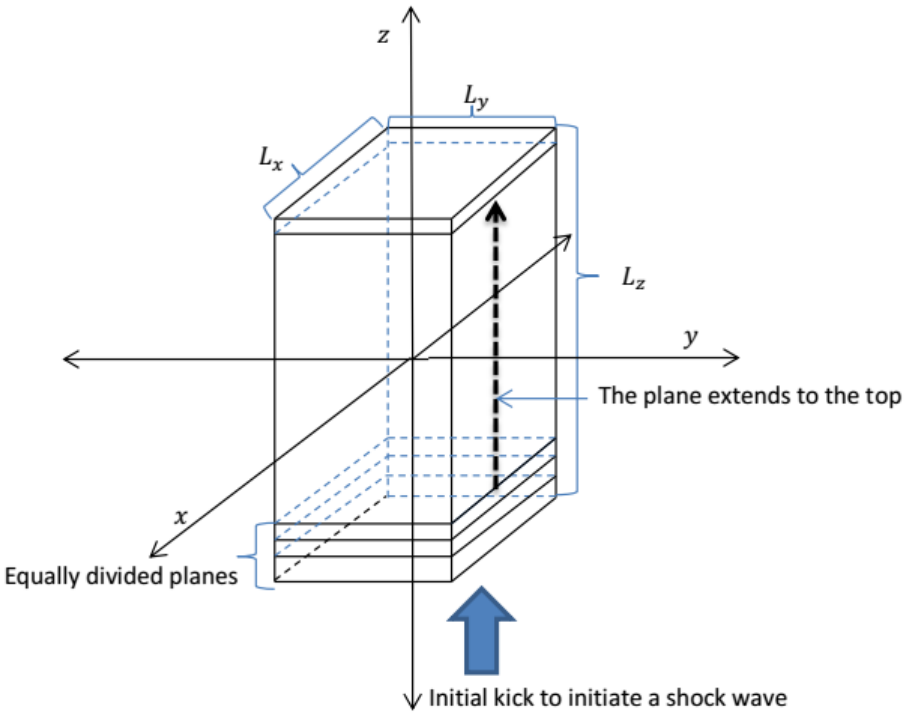

Figure 2.1: Schematic diagram of simulation setup.

2.2 Molecular dynamics

Throughout the simulation, we have considered spherical shaped particles of diameter (σ), while the interaction between particles is taken to be a simple Lennard-Johns$(12-6)$ potential $(\phi_{LJ}(r))$. However, the potential is truncated and shifted for the following reasons. First, for a system of N particles, computing the full potential $(\phi_{LJ}(r))$ is an $O(N^2)$ process whenever all particles interact. In practice, the interactions are negligible at long distances, however, and for this reason, one always introduces a cut-off at some interparticle distance $r = r_c$ beyond which interactions are ignored; besides, this makes the force calculation almost $O(N)$ process [43]. Secondly, to avoid a discontinuity in the energy at the potential cut-off, a constant shift can be added to the potential so that the energy at the cut-off boundary becomes zero. As a result, phenomenological form of the potential due to neutral molecules is given by:

$$\phi_{LJ}(r) = 4\varepsilon\left(\left(\frac{\sigma}{r}\right)^{12} - \left(\frac{\sigma}{r}\right)^{6}\right) \tag{2.1}$$

Here r is the inter-particle separation, ε is the energy well depth and σ represents the length parameter. Next, the truncated and shifted potential takes the form as follows:

$$\phi_{TSLJ}(r) = \begin{cases} \phi_{LJ}(r) - \phi_{LJ}(r_c), & \text{if} r \leq r_c \\ 0, & \text{if} r > r_c \end{cases} \tag{2.2}$$

Where r_c signifies the cut-off radius. In our simulation we used a cut-off radius of $r_c = 2^{1/6}\sigma$. To simulate the dynamics of interacting particles, the equation of motion was integrated using Velocity-Verlet algorithm [44, 45]. Moreover, in a classical Molecular dynamics simulation, the most crucial part of the computation is force calculation. One can calculate it from the gradient of potential function [45].

$$\vec{F}(r) = -\vec{\nabla}\phi_{LJ}(r) \tag{2.3}$$

According to the Velocity-Verlet algorithm, the position is expanded to the second order of infinitesimal time step δt, using the Taylor series. Hence, the position of a given particle at a later time is:

$$\vec{r}(t+\delta t) = \vec{r}(t) + \delta t\dot{\vec{r}}(t) + \frac{\delta t^2}{2}\ddot{\vec{r}}(t) \tag{2.4}$$

Additionally, the velocity vector at a time $t+\delta t$ is given by:

$$\vec{v}(t+\delta t) = \vec{v}(t) + \frac{\delta t}{2}\left(\dot{\vec{v}}(t) + \dot{\vec{v}}(t+\delta t)\right) \tag{2.5}$$

Obviously, the first derivative of position vector is velocity, $\dot{\vec{r}} = \vec{v}$, and also the second derivative gives the acceleration, $\ddot{\vec{r}} = \vec{a}$. From Newton's second law of motion, one can find the acceleration, $\vec{a} = \vec{F}/m$, where m stands for the mass of the particle. In the simulation code, the velocity is integrated into two parts, primarily after the force is being calculated at t, i.e., $\vec{F}(t)$, secondly, after the computation of $\vec{F}(t+\delta t)$.

2.3 Physical quantities and their reduced forms

Subsequently, the previous kinematics and dynamical analysis on particles' enabled us to compute some statistical variables, such as kinetic temperature, pressure, and total energy of the system. The pressure of the system is computed using the virial expression [46].

Table 2.1: L-J parameters for Neon.

Atom	$\sigma(10^{-10}m)$	$\varepsilon\ (10^{-23}J)$	m$(10^{-26}kg)$
Neon	2.72	64.86	3.35

Table 2.2: Lennard-Johns scales for a few physical quantities.

Physical quantities	Formula	L-J scale
Time (τ)	$\sqrt{m\sigma^2/\varepsilon}$	$1.95\times10^{-12}sec$
Speed (v)	$\sqrt{\varepsilon/m}$	$139.14m/s$
Density (ρ)	m/σ^3	$1,664.7kg/m^3$
Temperature (T)	ε/k_b	$47.0K$
Pressure (P)	ε/σ^3	$32.7MPa$

$$P=\frac{2}{3V}\langle E_{kin}\rangle+\frac{1}{3V}\sum_{i=1}^{n}\sum_{j\neq i}^{n}(\vec{r}_i-\vec{r}_j).\vec{F}_{ij} \tag{2.6}$$

Here $\langle E_{kin}\rangle$ denotes the average kinetic energy, and V depicts the system's volume with n number of particles. In MD simulation, one can calculate the temperature using the average kinetic energy of the system [47], which is

$$T=\frac{2}{3k_B}\langle E_{kin}\rangle. \tag{2.7}$$

Given that

$$\langle E_{kin}\rangle=\frac{1}{2}m\langle v^2\rangle, \tag{2.8}$$

where k_b is the Boltzmann constant. While the mean square speed $\langle v^2\rangle$ is expressed as:

$$\langle v^2\rangle=\frac{1}{n}\sum_{i=1}v_i^2. \tag{2.9}$$

In doing so, we have used a typical Lennard-Johns fluid composed of neon atoms. We choose such an atom because water and neon are found to be isoelectronic [48]. Besides, their masses are closer to each other. Consequently, this investigation may well be supplementary for underwater shock wave studies on a large scale. Then, the L-J parameters for neon atom according to [49] is shown in Table 2.1.

Based on provided parameters, the L-J scale of some physical quantities is listed in Table 2.2. Additionally, throughout this numerical investigation, we have expressed all physical

Table 2.3: Physical quantities and their reduced units.

Physical quantities	Reduced unites
Time	$\tau^* = \sqrt{\varepsilon/(m\sigma^3)}\tau$
Length	$r^* = r/\sigma$
Speed	$v^* = \sqrt{m/\varepsilon}v$
Density	$\rho^* = \rho\sigma^3/m$
L-J potential	$\phi^*_{LJ} = \phi_{LJ}/\varepsilon$
Pressure	$P^* = P\sigma^3/\varepsilon$
Temperature	$T^* = Tk_b/\varepsilon$

quantities in suitable reduced units to avoid a numerical error due to minimal values of molecular mass, inter-molecular distance, and time interval at the molecular level. For this reason, some of the physical quantities and their reduced units are expressed in L-J scales, see Table 2.3. Thus, we see that the reduced physical quantities are dimensionless. Further, in the simulation, we used a reduced time step of $\delta\tau^* = 0.005$, and a density of the L-J fluid is taken to be $\rho^* = 0.6$.

2.4 Techniques of computation

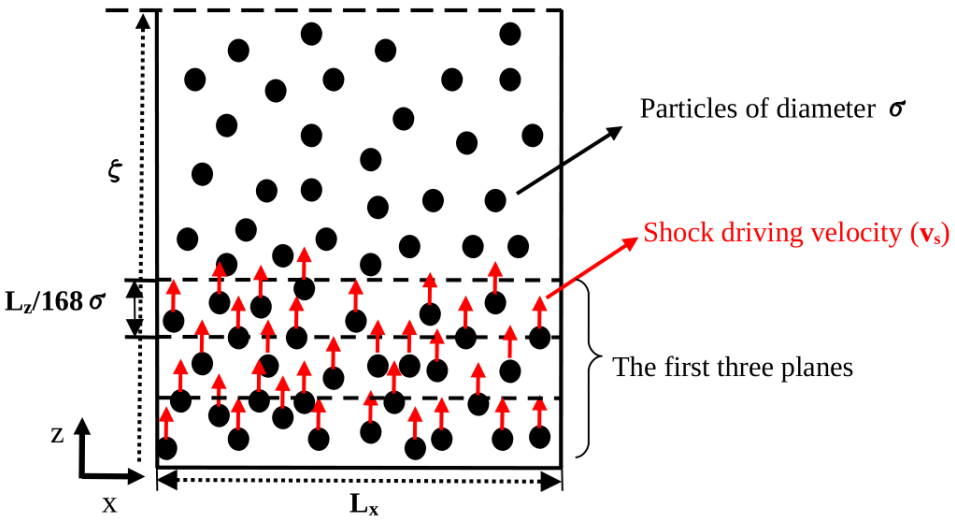

Figure 2.2: A two dimensional schematic diagram of shock wave generation at the bottom of simulation box.

Afterward, the system was thermally equilibrated before shock wave generation; this

is done by re-calibrating each particle's velocity according to the working temperature. After all of these initialization, a shock wave generation and the subsequent propagation have been studied using the thermal-impulsive technique. In this method, particles in the first three planes are given an initial shock-driving speed (v_s) toward the positive $z-$direction, see Figure 2.2. As a result, there will be an increment in the system's kinetic temperature when initial input energy is given to the system via an incident shock wave. Meanwhile, we have investigated the shock signal by measuring either the particles' displacement along the z-axis as a function of time or the local pressure variation due to perturbation propagation. First, the particles' displacement measurements and local pressure are conducted at specific locations along the z-axis. More specifically, a plane of $L_z/168\sigma$ thickness and perpendicular to the $z-$axis is selected at a distance ζ from the source. Next, the average displacement of all particles within a preference plane is computed to find the displacement pulse-amplitude (Δz) of a shock wave. Following that, the local pressure of a given plane is calculated. Then, the ambient pressure of the system is subtracted from it to find the pressure pulse-amplitude (ΔP_a).

3
Results and Discussion

First, we have investigated the temporal variation of both pressure and displacement pulse for initial shock driving speed of $v_s = 22.0$ and $v_s = 16.0$. Accordingly, we have selected five distinct planes at a distance ζ from the shock source. Then the displacement of a given plane is computed by averaging the z-component of particle displacement in each time step. Accordingly, the time evolution of local pressure of the corresponding planes is calculated by calculating the virial of every particle within the same plane. The results have been averaged over 20 number of runs, accordingly. Afterward, the output is depicted in Figure 3.1. The left and right side of the curves correspond to the perturbation front and rear, respectively. Indeed the temporal variation of local pressure in Figure 3.1c is found to be similar with shock wave structures which were measured using PCB138 and Müller-plate pressure probes in a micro-second time scale [15], correspondence in the pressure waveform also observed in experimental results of recent articles [39–41].

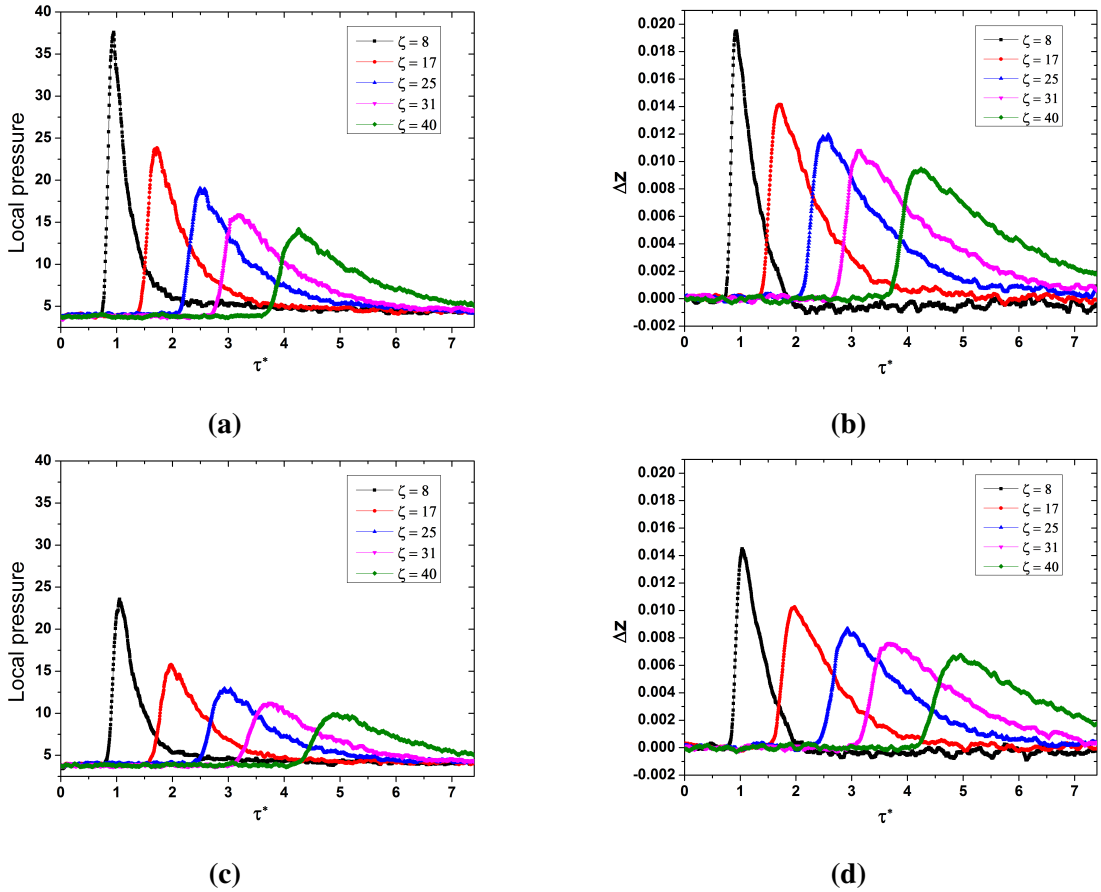

Figure 3.1: Temporal variation of local pressure and displacement pulse-amplitude for shock-driving velocity for $v_s = 22.0$ [(a) and (b)] and for $v_s = 16.0$ [(c) and (d)], respectively. The plot is taken for five different planes at a distance ζ from the shock source.

Further, we see that the traveling shock wave signal exhibits a short rise time and slow decays at a given point. The reason for a quick rise is that the shock front travels at a higher speed; thus, the incident traveling wave transfers a higher momentum to particles in a particular plane; hence particles become quickly packed with their neighbor ones. Consequently, their repulsive potential escalates, and this gives rise to the rapid increase of local pressure. Secondly, the rapid growth of displacement pulse-amplitude of a given cell is seen. The reason is, as the traveling shock signal interacts with a given particle, the subject particle is displaced long enough in proportion to the transferred momentum to it. Secondly, we know that a wave's speed is greater than the speed of diffusive particles in any medium. Hence, after a shock wave passes by a given point, particles begin to diffuse toward a less dense zone. As a result, the local pressure decays slowly and also the displacement of individual particles. Generally speaking, the quick rise and slow fall of a shock wave are due to shock front and diffusion of particles, respectively. The fluid's

viscosity contributes a significant role in the dissipation of the signal's energy as the pulse travels through the medium. Thus, One can see a loss of sharpness of a traveling wave characterized by a decrease of peak and broadening as the perturbation travels through the medium. Moreover, the pulse posses a triangular shape as we go further from the source. Correspondingly, a similar result has been found in some experimental investigations of shock wave [15, 50, 51].

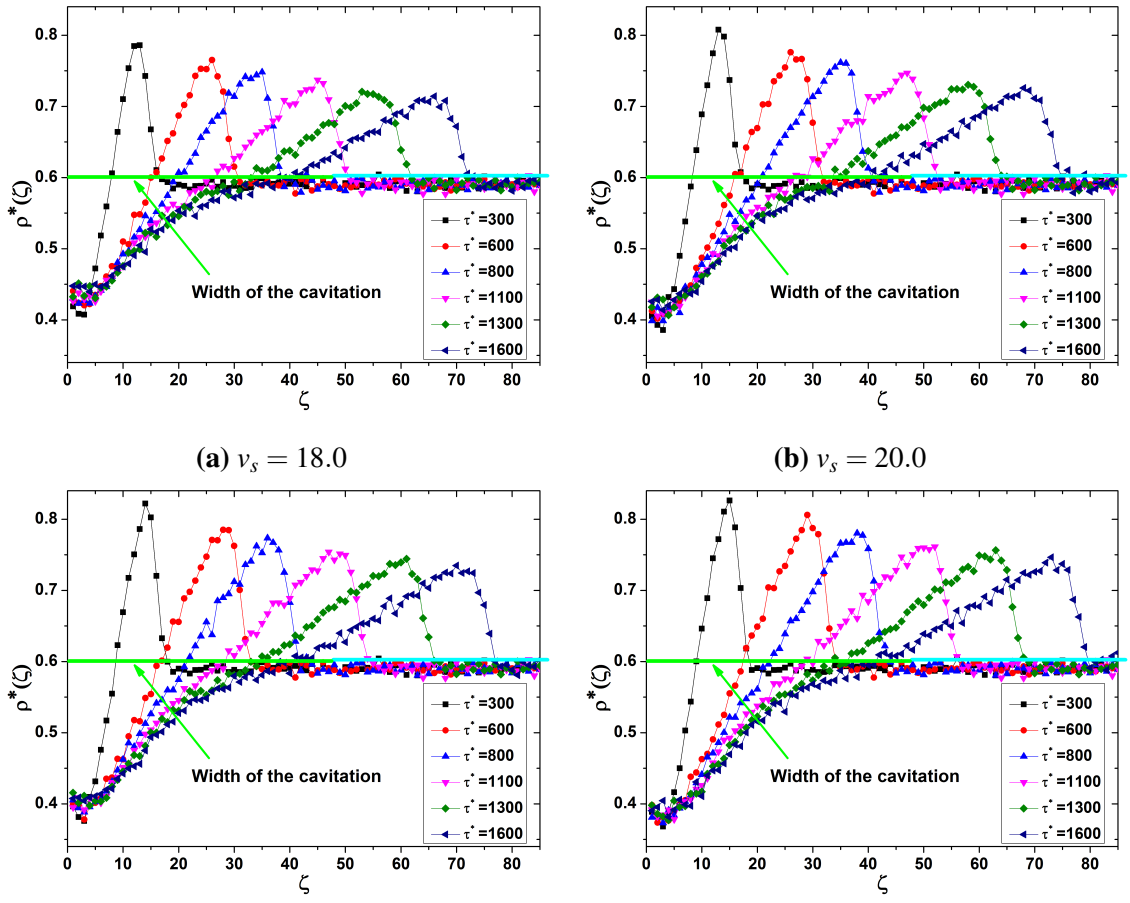

(a) $v_s = 18.0$ **(b)** $v_s = 20.0$

(c) $v_s = 22.0$ **(d)** $v_s = 24.0$

Figure 3.2: Density profile of a traveling shock wave for four different shock driving speed.

Moreover, from Figure 3.2 we see that during the early stage of shock wave propagation a cavity of lower density is formed. Due to a higher shock driving speed, the temperature increases drastically near by the bottom of the box, this leads to a rapid increase in the volume of the cavity. Consequently, a significant compression of the fluid and thereby a shock wave is generated. Accordingly, the rapid expansion of the cavity is

accompanied by a highly compressed layer of the fluid. Thereafter, the expansion of the cavity decreases as time goes by. The green line in the graph depicts width of the cavity. Further, one can see from the previous plot that at a later time, the shock wave departs from the cavity and travels as a sound wave pulse. Generally, the generation of the shock wave occurs because of the formation of the compressed fluid layer near the shock source by the cavity expansion.

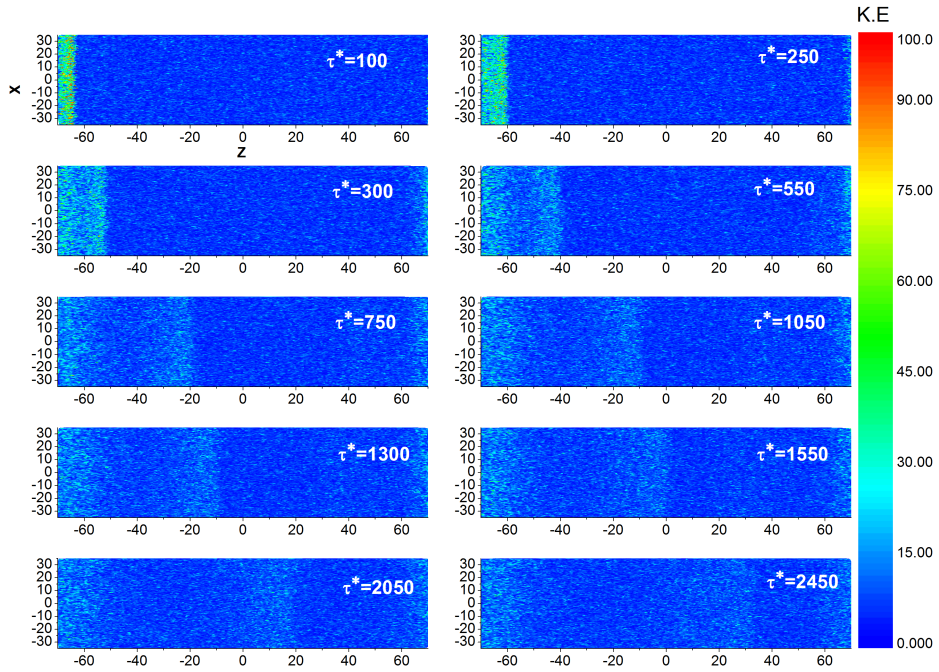

Figure 3.3: Snapshots of progressive simulation by particles kinetic energy at different reduced time (τ^*).

We have taken the snapshot of shock wave propagation throughout this investigation according to particles' kinetic and potential energy for the first $2,450$ reduced times at different intervals. In doing so, from Figure 3.3 and 3.4 we see that the traveling pulse poses a narrow, sharp, and highly peaked shape at the beginning of propagation. However, as time goes on, it dissipates most of its kinetic and potential energy and attenuates to the least amount of energy. For a rapid loss of potential and kinetic energy, the fluid's viscosity could be taken as a primary cause besides other unknown factors that could trigger the propagation. Moreover, from Figure 3.3 we observe that the temperature gradient estab-

lished would not propagate by diffusion alone as in heat conduction; however, it would propagate like a wave with a certain velocity. Besides, due to the cavity formation nearby the shock source some of incident energy is deposited in the early stage of propagation, see Figure 3.3.

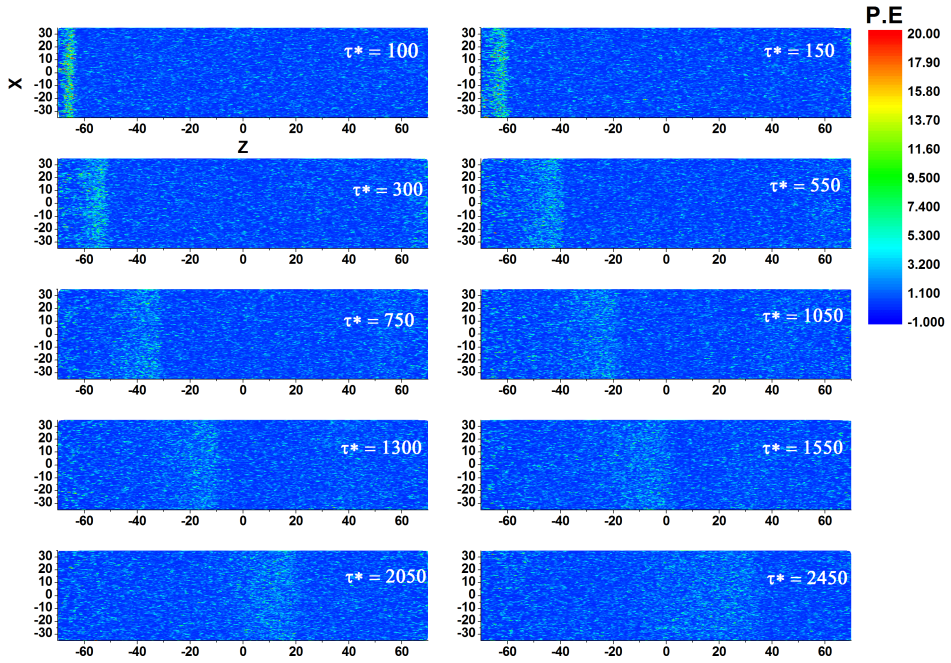

Figure 3.4: Snapshots of progressive simulation by particles potential energy at different reduced time (τ^*).

Next, the spatial variation of shock wave amplitude is measured as a function of distance ζ using both local pressure and displacement pulse-amplitude, see Figure 3.5. Regardless of the shock driving speed, the amplitude of shock waves drops rapidly and attenuates nearly to the same level. One may also see a rapid decay of traveling pulse's amplitude in some of previous shock wave investigations [1, 2, 15, 16]. The reason for a rapid drop in the pressure amplitude is because the energy is dissipated as a shock wave travels throughout a fluid. Correspondingly, the wave's kinetic and potential energy also dissipates spatially; see Figure 3.3 and 3.4.

To investigate the convergence of decaying amplitude, we plotted the logarithm of

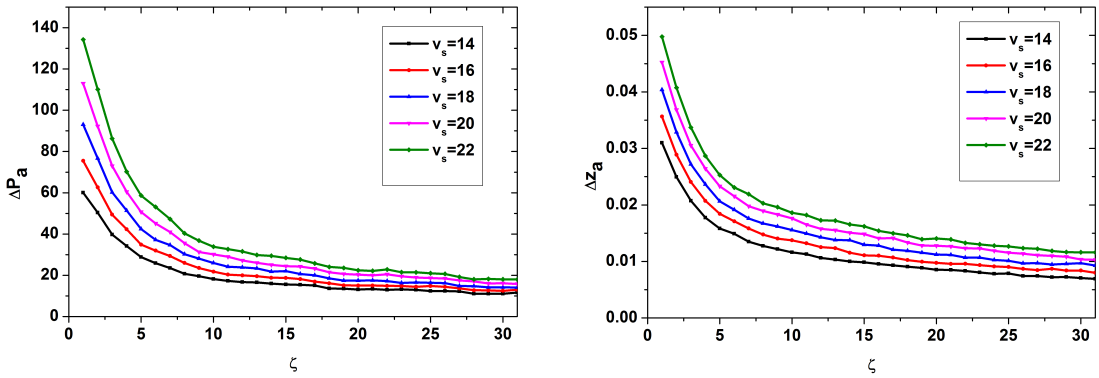

(a) **(b)**

Figure 3.5: The amplitude of pressure and displacement pulse as a function ζ (distance from the source). (a) Spacial variation of pressure pulse-amplitude for different shock driving speed v_s. (b) Spatial variation of local Displacement amplitude of particles for five v_s.

pressure and displacement pulse amplitude ($ln\Delta P_a, ln\Delta z_a$) to the logarithm of distance (ζ). The linearity of the graph tells us that the pressure and displacement pulse-amplitude demonstrably converge to a power function; see Figure 3.6. Accordingly, we can say that the amplitude of both pressure and displacement pulse is proportional to the power of distance ζ, that is, $\Delta P_a \sim \zeta^m$ and $\Delta z_a \sim \zeta^m$, respectively. Moreover, to see the future history of the decaying amplitude, we have modeled a power function to both pressure and displacement pulse-amplitude decay for a shock driving velocity of $v_s = 18.0$, see equation (3.1) and (3.2) bellow:

Pressure pulse-amplitude as a function of distance from the source:

$$\Delta P_a(\zeta) = A\zeta^m \tag{3.1}$$

Displacement pulse-amplitude as a function of distance from the source:

$$\Delta z_a(\zeta) = B\zeta^m \tag{3.2}$$

Where A, B, and m are constants to be determined. As we see Figure 3.7a and 3.7b, the data plot is well-matched with the proposed functions. Hence, from the result, we can infer that the data plot in a black dot is found to be well fitted with the power function curve in red and blue line for both pressure and displacement amplitude, respectively. From the fitting analysis, the corresponding constants are listed in Table 3.1. We can

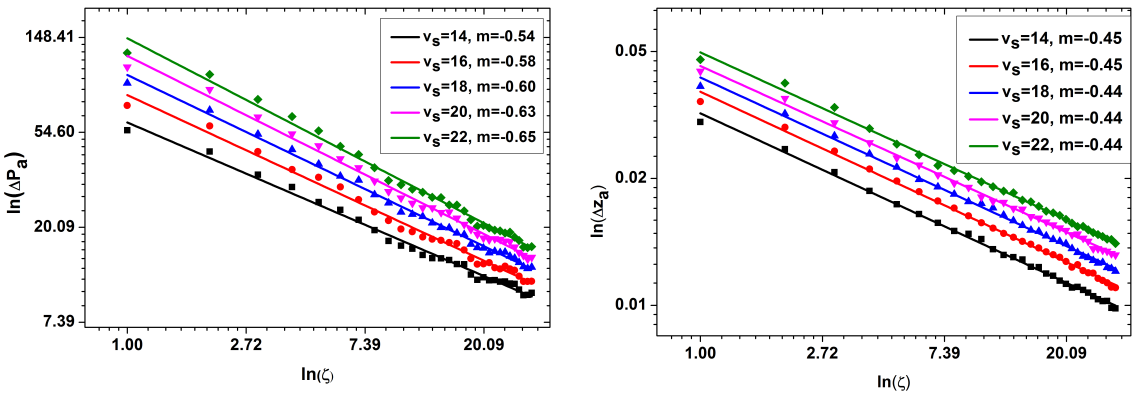

(a) **(b)**

Figure 3.6: The logarithm plot of shock wave amplitude for five distinct v_s, where m is the slop. (a) Logarithm of pressure pulse-amplitude ($ln(\Delta P_a)$) versus logarithm of distance from the source ($ln\zeta$). (b) Logarithm of displacement pulse-amplitude ($ln(\Delta z_a)$) versus logarithm of distance from the source ($ln\zeta$).

Table 3.1: Parameters of Decaying amplitude for shock driving velocity of $v_s = 18.0$.

Pressure pulse-amplitude	Displacement pulse-amplitude
$A = 99.48$	$B = 0.04$
$m = 0.60$	$m = 0.44$

see that for a long enough distance from the shock wave origin ($\zeta \to \infty$), the pressure pulse-amplitude diminishes ($\Delta P_a \to 0$). However, the local pressure of a particular plane will be equal to the ambient pressure of the system, see Figure 3.1. Likewise, the same approximation is also made for spatial variation of displacement pulse-amplitude within the same limit. For a much further distance ($\zeta \to \infty$) the displacement pulse-amplitude vanishes ($\Delta z_a \to 0$). As a result, we can deduce that the system tends to equilibrate itself after the perturbation is ceased.

The temporal variation of shock wave position from the source is plotted in black dot, see Figure 3.8a and 3.8b for pressure and displacement pulse, respectively. The trajectory has been taken by tracking the shock pulse as it covers a distance ζ within a time of τ^*. Afterward, by taking the derivative of the distance-time fitting curve, one can get the velocity of a shock wave in time. As a result, the red and blue plots in Figure 3.8c, and Figure 3.8d are the temporal variation of shock velocity for both pressure and displacement wave pulses, respectively. We see that the velocity of shock pulse drops very quickly

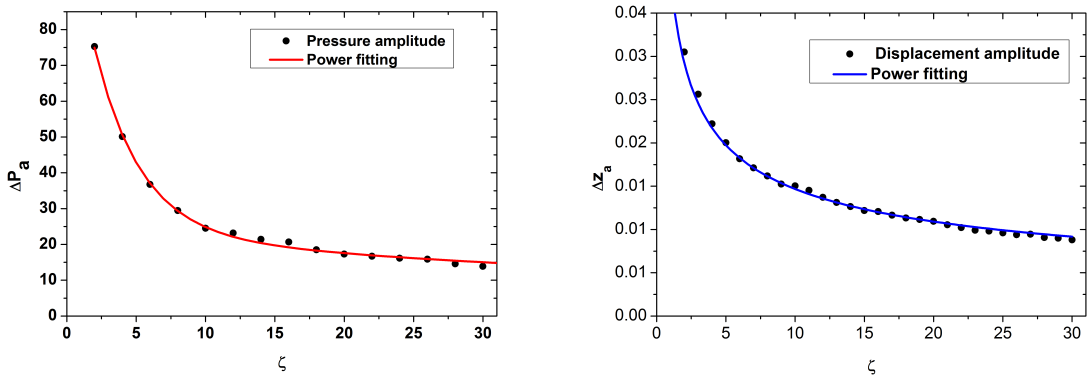

(a) **(b)**

Figure 3.7: Pressure and displacement amplitude for shock-driving velocity of $v_s = 18.0$. (a) Spatial variation of pressure pulse-amplitude as a function of ζ (distance from the source). (b) Spatial variation of displacement pulse-amplitude as a function of ζ (a distance from the source).

from the two plots, which is expected for shock waves traveling through any medium. Interestingly, a similar characteristic curve in the evolution of shock wave velocity had been observed in an underwater shock wave caused by an electrical explosion, see [17, 42]. A further similar result also found for a shock wave emission by cavitation collapse, in a nano time scale [15]. Evidently, the theoretical calculation for a spherical shock wave also gives the same decaying velocity of propagation [52]. In-depth discussion and analysis are made in the listed articles on their accord. Accordingly, a detailed theoretical analysis was also made in article [53].

According to our simulation result, the speed of shock wave propagation in Figure 3.8c and 3.8d drops from $v^* \sim 28.0$ $(3,895.92\ m/s)$ at $\tau^* \sim 0.5$ $(0.98\ ps)$ to $v^* \sim 7.6$ $(1,057.46\ m/s)$ at $\tau^* \sim 7.8$ $(15.21\ ps)$ for pressure pulse, and $v^* \sim 29.1$ $(4,048.97\ m/s)$ at $\tau^* \sim 0.5$ $(0.98\ ps)$ to $v^* \sim 7.5$ $(1,043.55\ m/s)$ at $\tau^* \sim 7.9$ $(15.41\ ps)$ for displacement pulse, respectively. One can see that during the first instant of shock wave propagation, the velocity of shock pulses is found to be extremely high, and it decays very quickly at a nearby distance from the source. Consequently, the velocity asymptotically falls back to the speed of sound in the respective medium; likely, a similar result is found in [1, 2]. During the early stage of shock wave generation, the cavity expands very quickly. Hence, the cavity pushes the fluid layers, supplying the shock with additional energy. Additionally, the cavity expansion with increasing velocity leads to further fluid layer compression, which propagates through the compressed fluid with a velocity larger than the velocity of

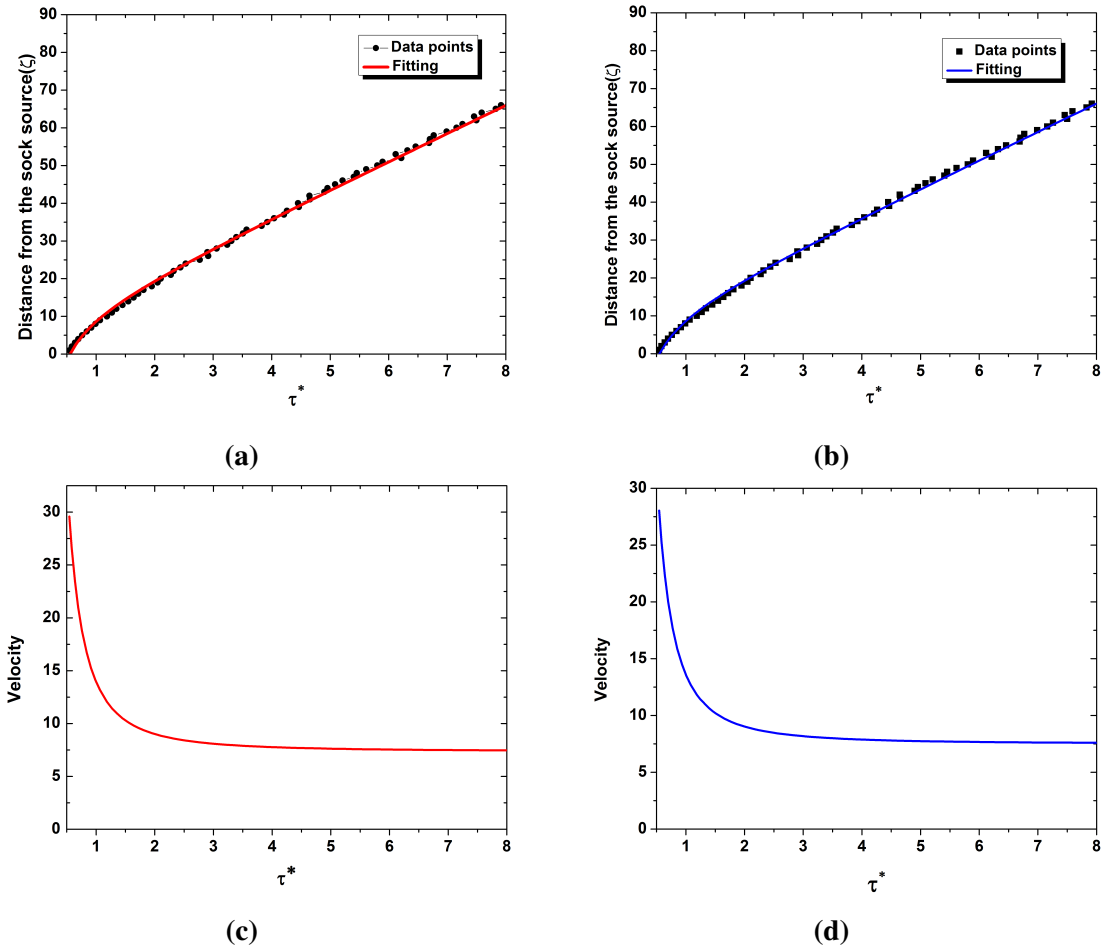

Figure 3.8: Trajectory and Velocity of the shock-pulse as a function of time for pressure pulse [(a) and (c)] and displacement pulse [(b) and (d)].

sound in undisturbed fluid. Due to the termination of energy deposition nearby the shock source, the expansion velocity of the cavity starts to decrease. Consequently, the generated shock pulse begins to drop its velocity in a quick manner. Moreover, the medium's viscosity creates a huge amount of friction for a shock-pulse to travel through. Hence, the shock wave is heavily dragged by the fluid and will eventually attain a terminal velocity, which is the speed of sound in the respective medium.

We have calculated the pressure and temperature of our system from the virial expression (2.6) and kinetic theory (2.7), respectively. The blue one represents pressure and the black for temperature, see Figure 3.8. The temperature curve rapidly increased and peaked at a maximum value at a moment of perturbation, while the pressure raised up and slowly increased as the temperature descends. The quick change of temperature resulted from the sudden increase in kinetic energy of the system as particles get a transfer of mo-

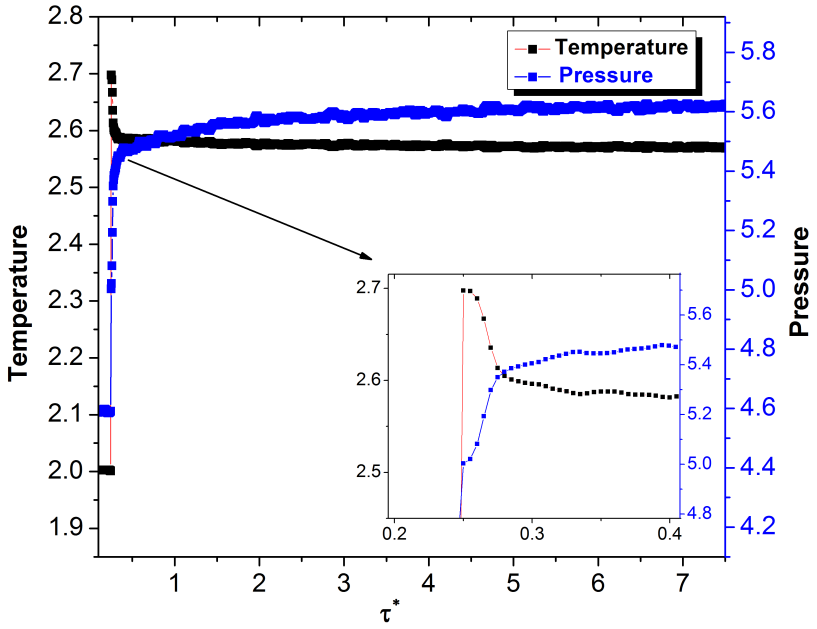

Figure 3.9: Evolution of pressure and temperature of the system at later reduced time τ^*.

menta from the bottom of the simulation box with a shock driving velocity of v_s. Besides, one may also see the quick change in the pressure; this is because in the virial expression (2.6), pressure is partially dependent upon the system's kinetic energy. Then, the pressure increases in proportion to a decreasing temperature due to the transfer of kinetic energy to potential energy. Meanwhile, the temperature is distributed to the system and dipped to a more significant value than the initial temperature, and stayed constant. This time the pressure of the particles rose slightly and maintained the same level when the system gets equilibrated. The system isolated energy is transferred from one form to another as the perturbation energy is slowly distributed to the particles because of energy conservation.

4
Conclusion

In summary, we have carried a three-dimensional Molecular dynamics simulation of a shock wave in L-J fluid. The shock signal has been investigated using both local pressure variation and average displacement of particles. A planar perturbation technique is employed to compute the temporal and spatial variation of shock signals. Accordingly, the amplitude and velocity of a shock wave have also been studied both in space and time, respectively. We have found that a planar shock wave decreases in strength with distance from the shock source, rapidly leveling out to a speed of sound. Furthermore, a correspondence between some experimental and simulation results has been found. Although most of the experiments were undertaken on a substantially larger scale, a striking resemblance with our result is observed. Our investigation tells us that if there could be a possibility of generating and propagating shock waves on such a minute scale, a similarity could be obtained in both experimental and simulation results. Besides, this day the rapid advancement of nanotechnology promises us in the future, there could be Nano-boats, which are capable of swimming in the blood vessels. Remarkably, a recent study has been able to achieve Nano-boats of micro-size [54]. With the aid of these tiny machines, perhaps one day, we may generate nano-shock waves. Mainly, medical science in synergy with nanotechnology would build such a machine for the treatment of incurable diseases like cancers, viruses, and many others. A group of nanobots may generate a very energetic

shock in a few tens of nano-meter away from a particular target cell or virus and could destroy the structure once and for all. The present work will be a good tool if someone inquires to design a nanobot capable of the previous function. It provides some statistical information regarding how pressure and temperature behave when an external shock is introduced into the medium.

Bibliography

[1] A. Doukas, A. Zweig, J. Frisoli, R. Birngruber, T. Deutsch, Non-invasive determination of shock wave pressure generated by optical breakdown, Applied Physics B 53 (4) (1991) 237–245.

[2] T. Juhasz, G. A. Kastis, C. Suárez, Z. Bor, W. E. Bron, Time-resolved observations of shock waves and cavitation bubbles generated by femtosecond laser pulses in corneal tissue and water, Lasers in Surgery and Medicine: The Official Journal of the American Society for Laser Medicine and Surgery 19 (1) (1996) 23–31.

[3] R. Pecha, B. Gompf, Microimplosions: cavitation collapse and shock wave emission on a nanosecond time scale, Physical review letters 84 (6) (2000) 1328.

[4] J. H. Lee, The detonation phenomenon, 2008.

[5] P. O. Krehl, History of shock waves, explosions and impact: a chronological and biographical reference, Springer Science & Business Media, 2008.

[6] J. J. Govoni, M. A. West, L. R. Settle, R. T. Lynch, M. D. Greene, Effects of underwater explosions on larval fish: implications for a coastal engineering project, Journal of Coastal Research (24) (2008) 228–233.

[7] J. P. Furia, High-energy extracorporeal shock wave therapy as a treatment for insertional achilles tendinopathy, The American journal of sports medicine 34 (5) (2006) 733–740.

[8] Z.-H. Xu, Q. Jiang, D.-Y. Chen, J. Xiong, D.-Q. Shi, T. Yuan, X.-L. Zhu, Extracorporeal shock wave treatment in nonunions of long bone fractures, International orthopaedics 33 (3) (2009) 789–793.

[9] M. Thiel, Application of shock waves in medicine, Clinical Orthopaedics and Related Research® 387 (2001) 18–21.

[10] M. Sackmann, M. Delius, T. Sauerbruch, J. Holl, W. Weber, E. Ippisch, U. Hagelauer, O. Wess, W. Hepp, W. Brendel, et al., Shock-wave lithotripsy of gallbladder stones, New England journal of medicine 318 (7) (1988) 393–397.

[11] L. Gerdesmeyer, C. von Eiff, C. Horn, M. Henne, M. Roessner, P. Diehl, H. Gollwitzer, Antibacterial effects of extracorporeal shock waves, Ultrasound in medicine & biology 31 (1) (2005) 115–119.

[12] C. Horn, K. Mengele, L. Gerdesmeyer, R. Gradinger, H. Gollwitzer, The effect of antibacterial acting extracorporeal shockwaves on bacterial cell integrity, Medical Science Monitor 15 (12) (2009) BR364–BR369.

[13] C. Horn, L. Gerdesmeyer, C. von Eiff, R. Gradinger, H. Gollwitzer, Energy-dependent stimulatory and inhibitory effects of extracorporeal shock waves on bacteria and on gentamicin activity, Medical Science Monitor 15 (6) (2009) MT77–MT83.

[14] G. Jagadeesh, K. Takayama, Novel applications of micro-shock waves in biological sciences, Journal of the Indian institute of Science 82 (1) (2002) 49.

[15] H. Zhou, Y. Zhang, R. Han, Y. Jing, J. Wu, Q. Liu, W. Ding, A. Qiu, Signal analysis and waveform reconstruction of shock waves generated by underwater electrical wire explosions with piezoelectric pressure probes, Sensors 16 (4) (2016) 573.

[16] W. Chen, O. Maurel, C. La Borderie, T. Reess, A. De Ferron, M. Matallah, G. Pijaudier-Cabot, A. Jacques, F. Rey-Bethbeder, Experimental and numerical study of shock wave propagation in water generated by pulsed arc electrohydraulic discharges, Heat and Mass Transfer 50 (5) (2014) 673–684.

[17] A. Rososhek, S. Efimov, V. Gurovich, A. Virozub, S. Tewari, Y. E. Krasik, Evolution of a shock wave generated by underwater electrical explosion of a single wire, Physics of Plasmas 26 (4) (2019) 042302.

[18] A. Grinenko, V. T. Gurovich, Y. E. Krasik, A. Sayapin, S. Efimov, J. Felsteiner, Analysis of shock wave measurements in water by a piezoelectric pressure probe, Review of scientific Instruments 75 (1) (2004) 240–244.

[19] J. Bushnell, D. McCloskey, Thermoelastic stress production in solids, Journal of Applied Physics 39 (12) (1968) 5541–5546.

[20] A. Zweig, V. Venugopalan, T. Deutsch, Stress generated in polyimide by excimer-laser irradiation, Journal of applied physics 74 (6) (1993) 4181–4189.

[21] L. Yang, Stress waves generated in thin metallic films by a q-switched ruby laser, Journal of Applied Physics 45 (6) (1974) 2601–2608.

[22] R. Fabbro, J. Fournier, P. Ballard, D. Devaux, J. Virmont, Physical study of laser-produced plasma in confined geometry, Journal of applied physics 68 (2) (1990) 775–784.

[23] Y. Tagawa, S. Yamamoto, K. Hayasaka, M. Kameda, On pressure impulse of a laser-induced underwater shock wave, Journal of Fluid Mechanics 808 (2016) 5–18.

[24] E. Y. Lau, M. L. Berkowitz, E. Schwegler, Shock wave-induced damage of a protein by void collapse, Biophysical journal 110 (1) (2016) 147–156.

[25] U. Adhikari, A. Goliaei, M. L. Berkowitz, Mechanism of membrane poration by shock wave induced nanobubble collapse: A molecular dynamics study, The Journal of Physical Chemistry B 119 (20) (2015) 6225–6234.

[26] K. P. Santo, M. L. Berkowitz, Shock wave interaction with a phospholipid membrane: Coarse-grained computer simulations, The Journal of chemical physics 140 (5) (2014) 02B602_1.

[27] M. Koshi, H. Matsui, T. Saito, H. Nagoya, K. Takayama, Molecular dynamics simulation of shock waves in gas phase ar; bunshi doryokugakuho ni yoru kitai shogekiha no simulation, Kayaku Gakkaishi (Journal of the Japan Explosives Society) 55 (1994).

[28] W. G. Hoover, Structure of a shock-wave front in a liquid, Physical Review Letters 42 (23) (1979) 1531.

[29] B. L. Holian, C. Patterson, M. Mareschal, E. Salomons, Modeling shock waves in an ideal gas: Going beyond the navier-stokes level, Physical review E 47 (1) (1993) R24.

[30] M. Marciante, M. S. Murillo, Thermodynamic and kinetic properties of shocks in two-dimensional yukawa systems, Physical review letters 118 (2) (2017) 025001.

[31] V. V. Zhakhovsky, M. M. Budzevich, A. C. Landerville, I. I. Oleynik, C. T. White, From laminar to turbulent detonations in energetic materials from molecular dynamics simulations, in: Journal of Physics: Conference Series, Vol. 500, IOP Publishing, 2014, p. 172005.

[32] B. Holian, Molecular dynamics comes of age for shockwave research, Shock Waves 13 (6) (2004) 489–495.

[33] W. G. Hoover, C. G. Hoover, From hard spheres and cubes to nonequilibrium maps with thirty-some years of thermostatted molecular dynamics, The Journal of chemical physics 153 (7) (2020) 070901.

[34] M. G. Fröhlich, T. D. Sewell, D. L. Thompson, Molecular dynamics simulations of shock waves in hydroxyl-terminated polybutadiene melts: Mechanical and structural responses, The Journal of chemical physics 140 (2) (2014) 024902.

[35] J.-L. Shao, P. Wang, A.-M. He, S.-Q. Duan, C.-S. Qin, Atomistic simulations of shock-induced microjet from a grooved aluminium surface, Journal of Applied Physics 113 (15) (2013) 153501.

[36] T. C. Germann, B. L. Holian, P. S. Lomdahl, R. Ravelo, Orientation dependence in molecular dynamics simulations of shocked single crystals, Physical review letters 84 (23) (2000) 5351.

[37] K. Kadau, T. Germann, P. Lomdahl, B. Holian, F. Cherne, Atomistic simulations of shock-induced phase transitions, in: AIP Conference Proceedings, Vol. 706, American Institute of Physics, 2004, pp. 229–234.

[38] K. McLaughlin, I. Oleynik, S. Zybin, M. Elert, C. White, Molecular dynamics simulations of an anomalous response of diamond to shock compression, in: AIP Conference Proceedings, Vol. 955, American Institute of Physics, 2007, pp. 321–324.

[39] S.-W. Liu, Y. Liu, Y.-J. Ren, F.-C. Lin, H. Li, Y. Zhao, Analysis of shock wave induced by underwater pulsed discharge using discharge current interception, Journal of Applied Physics 127 (14) (2020) 143301.

[40] D. Tan, Reduced-order models of electrohydraulic pulsed discharge and concrete fracture, Ph.D. thesis, The Cooper Union for the Advancement of Science and Art (2020).

[41] S. Tanaka, I. Bataev, M. Nishi, I. Balagansky, K. Hokamoto, Micropunching large-area metal sheets using underwater shock wave: Experimental study and numerical simulation, International Journal of Machine Tools and Manufacture 147 (2019) 103457.

[42] A. Rososhek, S. Efimov, A. Virozub, D. Maler, Y. E. Krasik, Particularities of shocks generated by underwater electrical explosions of a single wire and wire arrays, Applied Physics Letters 115 (7) (2019) 074101.

[43] S. Toxvaerd, J. C. Dyre, Communication: Shifted forces in molecular dynamics, The Journal of chemical physics 134 (8) (2011) 081102.

[44] D. C. Rapaport, The art of molecular dynamics simulation, Cambridge university press, 2004.

[45] W. H. Gai, R. Guo, The basic theories of molecular dynamics simulation, in: Applied Mechanics and Materials, Vol. 444, Trans Tech Publ, 2014, pp. 1483–1488.

[46] E. van den Akker, A. Frijns, A. van Steenhoven, P. Hilbers, Thermodynamic analysis of molecular dynamics simulations of evaporation and condensation, molecules 1001 (2008) d2ri.

[47] M. Woo, I. Greber, Molecular dynamics simulation of piston-driven shock wave in hard sphere gas, AIAA journal 37 (2) (1999) 215–221.

[48] A. Bar-on, R. Naaman, Vibrational induced photodetachment of electrons from small clusters, The Journal of chemical physics 90 (9) (1989) 5198–5199.

[49] M. F. Pas, B. J. Zwolinski, Computation of the transport coefficients of dense fluid neon, argon, krypton and xenon by molecular dynamics, Molecular Physics 73 (3) (1991) 471–481.

[50] R. Han, H. Zhou, J. Wu, A. Qiu, W. Ding, Y. Zhang, Relationship between energy deposition and shock wave phenomenon in an underwater electrical wire explosion, Physics of Plasmas 24 (9) (2017) 093506.

[51] R. Han, H. Zhou, J. Wu, T. Clayson, H. Ren, J. Wu, Y. Zhang, A. Qiu, Experimental verification of the vaporization's contribution to the shock waves generated by underwater electrical wire explosion under micro-second timescale pulsed discharge, Physics of Plasmas 24 (6) (2017) 063511.

[52] K. Wen, X.-W. Chen, D.-N. Di, Modeling on the shock wave in spheres hypervelocity impact on flat plates, Defence Technology 15 (4) (2019) 457–466.

[53] S. G. Chefranov, Dissipative instability of shock waves, Journal of Experimental and Theoretical Physics 130 (2020) 633–642.

[54] M. Z. Miskin, A. J. Cortese, K. Dorsey, E. P. Esposito, M. F. Reynolds, Q. Liu, M. Cao, D. A. Muller, P. L. McEuen, I. Cohen, Electronically integrated, mass-manufactured, microscopic robots, Nature 584 (7822) (2020) 557–561.

Declaration

I declare that this thesis entitled **"Generation and Propagation of Nano Shock Waves in a Lenard-Johns Fluid"** is the result of my own research except as cited in the references. The thesis has not been accepted for any degree and is not concurrently submitted in candidature of any other degree.

Kidanemaryam Shambel

June, 2021